Journal of Alloys and Compounds 642 (2015) 148–152

Contents lists available at ScienceDirect

Journal of Alloys and Compounds

journal homepage: www.elsevier.com/locate/jalcom

Synthesis of carbon quantum dots and zinc oxide nanosheets by pyrolysis of novel metal–organic framework compounds

Qiliang Ma, Zhaochun Zhang *, Zhenwei Yu

Department of Electronic Information Materials, Shanghai University, Shanghai 200072, China

ARTICLE INFO

Article history:
Received 15 December 2014
Received in revised form 24 February 2015
Accepted 15 April 2015
Available online 21 April 2015

Keywords:
Carbon quantum dots
Zinc oxide nanosheets
Metal–organic frameworks

ABSTRACT

Here, the carbon quantum dots and zinc oxide nanosheets with novel superstructures are successfully synthesized simultaneously from a hydrothermal preparation and thermal decomposition of a porous precursor of metal–organic frameworks. Porous metal–organic frameworks are prepared by the hydrothermal process by using zinc nitrate hexahydrate, 4,4′-oxybisbenzoic acid and 4,4′-bipyridine as the starting materials. Fluorescence spectrophotometer, X-ray powder diffraction, transmission electron microscopy and high-resolution transmission electron microscopy were used to characterize the structure and property. The results show the coexistence of carbon quantum dots and zinc oxide nanosheets. The carbon quantum dots size is about 4 nm. Particularly, zinc oxide nanosheets show a new triangular sheet structure that has almost the same size. Strong ultraviolet emission of this coexistence system should be useful in developing visible light-emitting and nanophotonic devices.

1. Introduction

Due to their unique optical and electronic properties caused by the quantum confinement and edge effects, quantum dots (QDs) have attracted considerable interest for the promising candidates to replace the conventional phosphor materials [1–7]. Unlike the traditional semiconductor QDs based on metallic elements, such as CdS, CdSe, PbSe and Ag_2S that more or less suffer from the problems of toxicity, hydrophobicity and high cost, carbon quantum dots (CQDs) have great superiority of low toxicity, stable fluorescent performance, easy to be chemically modified, good compatibility with organic, inorganic and biological molecules [8,9]. Therefore, CQDs have been widely used in drug analysis, bio-labeling and medical field. Refer to the synthesis routes of CQDs, a variety of synthesis approaches including pyrolysis [10], electrochemical exfoliation [6,11–13], incomplete combustion oxidation [14], acidic oxidation [15], laser ablation [16], hydrothermal treatments [17], microwave/ultrasonic passivation [7,18], and plasma treatment [19] in recent years have been developed to prepare CQDs with various precursors (such as graphite oxide [20], citric acid [21], glycerol [22], coffee grounds [23], soy milk [24], grass [25], and egg [19]).

We selected the metal–organic frameworks (MOFs) that had not been reported as precursor of pyrolysis. MOF [26–28] is a kind of porous material, in which inorganic assemblies are joined by multitopic organic ligand. Because of the special structure of MOFs, we not only obtain CQDs, but also found that ZnO nanosheets. We know various ZnO nanostructures, including wires, belts, cables and tubes, combs, tetrapods, rings and disks, tower-like, rotor-like, flower-like [29,30], oriented helical nanorod arrays [31] and other complex nanostructures [32]. But, characterized by transmission electron microscopy (TEM), the ZnO nanosheets we prepared shows a new triangular sheet structure. Besides, CQDs and ZnO nanosheets formed a coexistence system. The study we using fluorospectrophotometer reveal coexistence system has strong ultraviolet emission. In general, not only CQDs, but also nano-ZnO has great superiority of low toxicity, stable fluorescent performance. Therefore, the coexistence system not only can be used to make biological fluorescence probe, but also have potential in developing visible light-emitting and nanophotonic devices.

2. Experimental

Firstly, 0.3 mol of 4,4′-oxybisbenzoic acid (OBA), 0.3 mol of zinc nitrate hexahydrate, and 0.3 mol of 4,4′-bipyridine were dissolved in a mixed solution of 10 mL of N,N-dimethyl-formamide and 5 mL of ethanol. The mixed solution was further magnetically stirred for 1 h, and then transferred into a Teflon-lined autoclave of 50 mL capacity. Put the autoclave at 359 K for 24 h. After being cooled to room temperature, white crystalline powder we obtained was washed several times with ethanol to remove the impurities and then dried at 333 K for 1 h. The crystal data of the white crystalline powder were collected by single crystal X-ray diffraction (SMART APEX II, BRUKER AXS GMBH) with $\omega = 2\theta$ at room temperature. The program of SAINT-5.0 and SHELXTL-97 were used for data reduction and structure analysis, respectively. Thermal analysis that in air atmosphere take heating rate of 15 K/min. The instrument is from NETZSCH Grinding & Dispersing.

* Corresponding author.
E-mail address: zhangzhaochun@shu.edu.cn (Z. Zhang).

http://dx.doi.org/10.1016/j.jallcom.2015.04.098
0925-8388/

Subsequently, put obtained white crystalline powder at 663 K for 2 h in a temperature-programmed Muffle furnace. After being cooled to room temperature, gray powders we obtained was characterized by XRD (D/MAX-RC model diffractometer) with the use of Cu Kα radiation (λ = 0.15418 nm). We first put the resulting gray powders into ethanol to ultrasound for 2 h, and then settling for twenty-four hour. The resulting supernatant is centrifuged and the precipitate removed. For transmission electron microscopy imaging of the structures, a drop of the resulting supernatant was put in a carbon-coated copper grid and dried in atmosphere. The several TEM images of samples were taken using a JEOLJEM-2100F microscope at the accelerating voltage of 200 kV. The supernatant were characterized for optical properties through a RF-5301PC fluorescence spectrometer (Shimadzu, Japan) and Leica DMIRB analysis was conducted on U-LH100HG. The preparation process is shown in Fig. 1.

3. Results and discussions

3.1. SC-XRD analysis of MOFs

Single crystal X-ray analysis revealed the following unit cell parameters. a = 16.77746(18) Å, b = 11.0642(12) Å, c = 22.440(2) Å, α = 90°, β = 90°, γ = 90°, V = 4164.8(8) Å^3, Z = 8. And the crystal system is orthorhombic, the space group is *Pcca*. Selected bond lengths and angles of the crystal are shown in Table 1.

The structure of the asymmetric unit is shown in Fig. 2a. In the asymmetric unit of compounds, including a six metal zinc coordination center, a 4,4′-oxybisbenzoic acid, a rigid 4,4′-bipyridine and an object of water molecules. In the structure, Zn1 form coordination bonds with the O1 of the carboxyl group and the N1 of 4,4′-bipyridine. Their bond lengths are 2.014(4) Å, 2.032(4) Å. The bond angle of N1–Zn1–O1 is 101.68(16)°. Fig. 2b shows a three-dimensional structure of the compound. Observing from the image of Fig. 2b, four oxygen atoms that coordinating to the zinc ion comes from different 4,4′-oxybisbenzoic acid. In the square pyramidal configuration of $ZnNO_4$, the nitrogen atom residing at axial vertices of square pyramidal, while four carboxyl oxygen atoms in the horizontal position. This structure not only containing organic molecules that capable of preparing carbon point, and can obtain ZnO by pyrolysis.

3.2. The thermokinetic analysis of the MOFs

The study of the MOFs is relevant to pyrolysis because decomposition these ligands occurs at different temperatures. Fig. 3a is the combined thermogravimetric analysis (TG) and derivative TG (DTG) profile showing the thermal degradation characteristics of MOFs at a heating rate of 15 °C min^{-1}. The pyrolysis process can be divided into two main regions: moisture and very light volatiles components removal (<250 °C); degradation of 4,4′-bipyridine (360–430 °C) and 4,4′-oxybisbenzoic acid decomposition (430–510 °C). Much of the devolatilization occurred in the second region of weight loss, a result of the thermal breaking of weak bonds in the porous structure of the constituent components of the MOFs and the formation of stronger, more stable bonds to take their place. Fig. 3b shows the Y–X curves at the first and second zone of the second region for the Freeman-Carroll's method. According

Table 1
Bond lengths [A] and angles [deg] for the compound.

Zn(1)–O(1)	2.014(4)	C(1)–O(2)	1.252(6)
Zn(1)–N(1)	2.032(4)	C(1)–O(1)	1.256(6)
Zn(1)–O(4)#1	2.032(4)	C(1)–C(2)	1.486(7)
Zn(1)–O(3)#2	2.037(4)	C(15)–N(1)	1.329(7)
Zn(1)–O(2)#3	2.044(4)	C(19)–N(1)	1.316(7)
O(4)–Zn(1)#6	2.032(4)	O(2)–Zn(1)#3	2.044(4)
Zn(1)–Zn(1)#3	2.895(10)	O(3)–Zn(1)#5	2.037(4)
N(1)–Zn(1)–O(3)#2	104.69(16)	O(1)–Zn(1)–N(1)	101.68(16)
O(4)#1–Zn(1)–O(3)#2	160.81(14)	O(1)–Zn(1)–O(4)#1	90.00(19)
O(1)–Zn(1)–O(2)#3	160.95(15)	N(1)–Zn(1)–O(4)#1	94.50(16)
N(1)–Zn(1)–O(2)#3	97.32(16)	O(1)–Zn(1)–O(3)#2	86.46(17)
O(4)#1–Zn(1)–O(2)#3	87.13(18)	O(4)#1–Zn(1)–Zn(1)#3	79.92(11)
O(3)#2–Zn(1)–O(2)#3	90.09(17)	O(3)#2–Zn(1)–Zn(1)#3	80.93(10)
O(1)–Zn(1)–Zn(1)#3	82.78(11)	O(2)#3–Zn(1)–Zn(1)#3	78.17(11)
N(1)–Zn(1)–Zn(1)#3	172.93(13)		

Symmetry transformations used to generate equivalent atoms: #1, $x-1/2$, $-y+1$, $-z+1/2$; #2, $-x+1/2$, y, $z-1/2$; #3, $-x$, $-y+1$, $-z$; #4, $-x+1/2$, $-y+2$, z; #5, $-x+1/2$, y, $z+1/2$; #6 $x+1/2$, $-y+1$, $-z+1/2$.

to nonisothermal kinetic theory, the thermal decomposition kinetic equation of solid-state material follows:

$$\frac{d\alpha}{dT} = \frac{A}{\beta}\exp\left(-\frac{E}{RT}\right)(1-\alpha)^n \tag{1}$$

where β is the constant heating rate (K/min), E is the activation energy (kJ/mol), A is the pre-exponential factor (s^{-1}), T is the absolute temperature (K), R is the universal gas constant (8.314 J mol^{-1} K^{-1}), and $(1-\alpha)^n$ is a reaction model function which has various forms depending on the physical mechanism. α is calculated from the TG curve:

$$\alpha = (m_0 - m)/(m_0 - m_\infty) \tag{2}$$

where m_0, m, and m_∞ are the initial, instantaneous, and final sample masses, respectively.

According to the Freeman-Carroll's method, we get

$$\frac{\Delta \log \frac{d\alpha}{dT}}{\Delta \log(1-\alpha)} = n - \frac{E}{2.3R}\cdot\frac{\Delta \frac{1}{T}}{\Delta \log(1-\alpha)} \tag{3}$$

Setting $Y = \frac{\Delta \log \frac{d\alpha}{dT}}{\Delta \log(1-\alpha)}$ and $X = \frac{\Delta \frac{1}{T}}{\Delta \log(1-\alpha)}$, then Eq. (3) can be put in the form

$$Y = n - \frac{E}{2.3R}\cdot X \tag{4}$$

The activation energy data, pre-exponential factor and order of reaction calculated from the Freeman-Carroll's method were collected in Table 2. The activation energy of process ② is higher than that of process ①, while the pre-exponential factor of process ② is smaller than that of process ①. The higher activation energy needs higher temperature, but also more sensitive to changes in temperature. Small pre-exponential factor shows that the number of low activity. From the thermokinetic analysis of the porous materials, it can be read that the thermal degradation of the materials was a

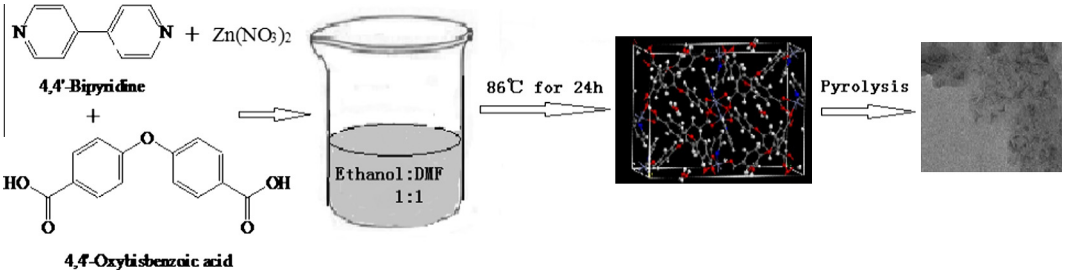

Fig. 1. The flow chart of the experiment.